

# RSC Advances



This is an *Accepted Manuscript*, which has been through the Royal Society of Chemistry peer review process and has been accepted for publication.

*Accepted Manuscripts* are published online shortly after acceptance, before technical editing, formatting and proof reading. Using this free service, authors can make their results available to the community, in citable form, before we publish the edited article. This *Accepted Manuscript* will be replaced by the edited, formatted and paginated article as soon as this is available.

You can find more information about *Accepted Manuscripts* in the [Information for Authors](#).

Please note that technical editing may introduce minor changes to the text and/or graphics, which may alter content. The journal's standard [Terms & Conditions](#) and the [Ethical guidelines](#) still apply. In no event shall the Royal Society of Chemistry be held responsible for any errors or omissions in this *Accepted Manuscript* or any consequences arising from the use of any information it contains.



Journal Name

Paper

## Defect Engineering Route to Boron Nitride Quantum Dots and Edge-Hydroxylated Functionalization for Bio-Imaging

Received 00th January 20xx,  
Accepted 00th January 20xx

DOI: 10.1039/x0xx00000x

www.rsc.org/

Jung-Hwan Jung,<sup>a</sup> Moumita Kotal,<sup>a</sup> Min-Ho Jang,<sup>b</sup> Junseok Lee,<sup>c</sup> Yong-Hoon Cho,<sup>b</sup> Won-Jong Kim<sup>c</sup> and Il-Kwon Oh<sup>a\*</sup>

Hexagonal boron nitride (h-BN) has considerable potential for applications owing to its attractive features including good thermal conductivity, chemical stability, and unique optical properties. However, because h-BN is chemically inert and thermally stable, it is hard to synthesize boron nitride quantum dots (BNQDs) using chemical methods such as oxidation, hetero-atom doping or functionalization. Here, we report a defect engineering method to synthesize BNQDs from h-BN using physical energy sources including an impinging process of heated iron nanoparticles, microwave irradiation and sonication. Furthermore, edge-hydroxylated functionalization was employed to enhance the intracellular uptake of the BNQDs in cells for bioimaging. The edge-hydroxylated BNQDs (EH-BNQDs) showed blue colored photoluminescence with 325 nm laser excitation, good cytotoxicity performance with approximately 100% cell viability, and a good attachment to cell surfaces. The successful endocytosis of EH-BNQDs using a cancer cell line was also demonstrated.

### Introduction

In the modern era of two-dimensional (2D) functional nanomaterials, hexagonal boron nitride (h-BN) has garnered considerable interest for potential applications in catalysts, optoelectronics, and semiconductor devices. h-BN is composed of layered structures held together by van der Waals forces, and it exhibits attractive features such as high dielectric property, high thermal conductivity, good chemical stability, and unique optical properties.<sup>1-9</sup> h-BN and graphite have almost identical values of mechanical strength and thermal conductivity, and have similar structures with a negligible difference of about 2% between their lattice constants. However, their electronic structures are totally different: graphene is a zero band gap semiconductor, while h-BN is a large band gap (~5.9 eV) insulator.<sup>10-12</sup> h-BN also has much stronger interactions between neighboring layers, and because of the ionic character of the B-N bond these interactions make it more difficult to form monolayer BN, compared to monolayer graphene.<sup>13,14</sup> Recently, graphene quantum dots (GQDs) have been

intensively investigated for various engineering applications including electrochemical sensors, photovoltaic devices, energy storage devices, and bio-sensors.<sup>15-20</sup> However, GQDs have been the subject of controversy regarding their toxicity and biocompatibility in bio-imaging and bio-sensor applications related to cell viability.<sup>21</sup> Generally, GQDs used for bio applications need to be carefully designed to reduce toxicity. In this respect, h-BN has much lower toxicity than graphene, better biocompatibility, has lower environmental hazard, and good cell viability. Consequently, if the BNQDs can be easily synthesized, boron nitride quantum dots (BNQDs) will be very suitable for bioimaging materials. However, because h-BN is chemically inert and thermally stable up to 1,000 °C,<sup>22</sup> it is very hard to synthesize BNQDs with nm dimensions with chemical methods such as oxidation, hetero-atom doping, intercalation, and functionalization.<sup>23,24</sup> Accordingly, very few studies regarding BNQDs are found in the open literature. Allwood *et al.* proposed a top-down approach involving potassium-intercalation and de-intercalation, and the disintegration of BN edges to form BNQDs.<sup>25</sup> Wu *et al.* prepared BNQDs *via* a facile sonication-solvothermal technique.<sup>26</sup> Moreover, to produce high-quality BNQDs for bioimaging, functionalization of the edge or surface of the BNQDs is crucial, not only for tuning the fundamental properties of the QDs, and rendering them stable and soluble in various aqueous environments, but also for creating good interactions with the cell surface for bioimaging. Hence, for bioimaging and biosensor applications, synthetic routes for the edge-functionalization of BNQDs need to be developed: this is a pending issue which has to be solved in the near future.<sup>27</sup>

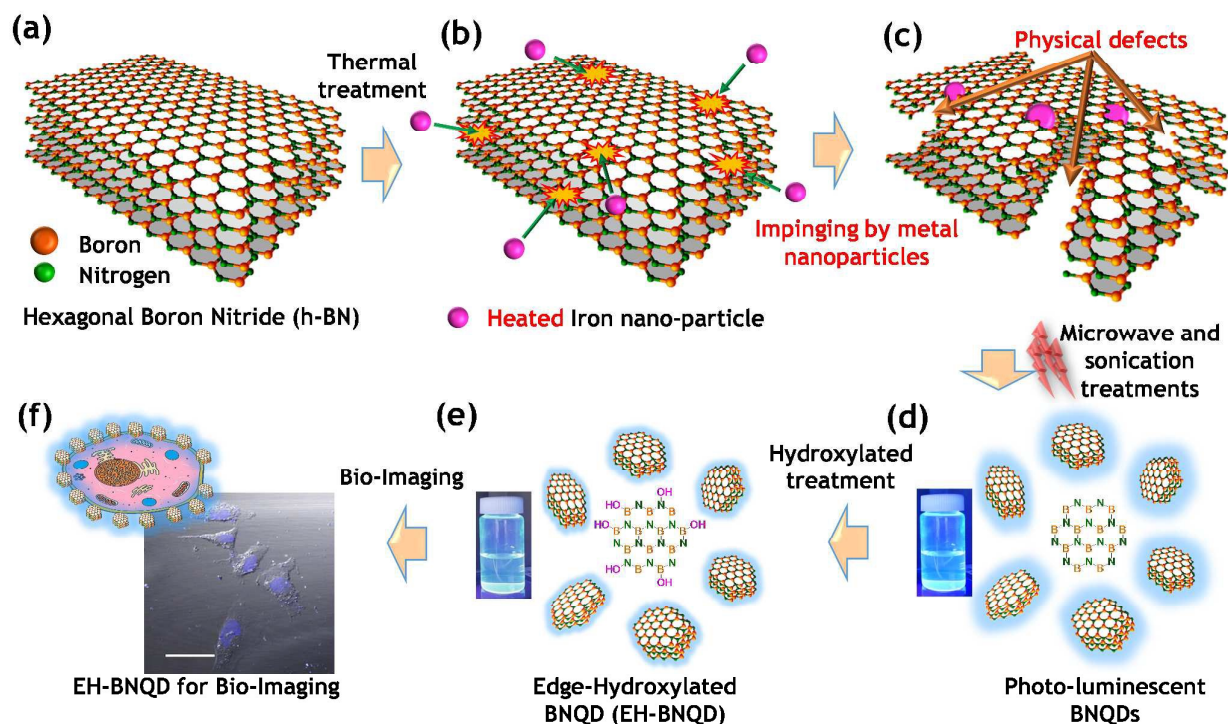
<sup>a</sup> Creative Research Initiative Center for Functionally Antagonistic Nano-Engineering, Department of Mechanical Engineering, Korea Advanced Institute of Science and Technology (KAIST), 291 Daehak-ro, Yuseong-gu, Daejeon 34141, Republic of Korea

<sup>b</sup> Department of Physics, Korea Advanced Institute of Science and Technology (KAIST), 291 Daehak-ro, Yuseong-gu, Daejeon 305-701, Republic of Korea Address here.

<sup>c</sup> Center for Self-assembled Complexity, Institute of Basic Science (IBS), and Department of Chemistry, Pohang University of Science and Technology (POSTECH), Pohang 37673, Republic of Korea

\* Corresponding author

Electronic Supplementary Information (ESI) available: supporting figures and table as described in the text. See DOI: 10.1039/x0xx00000x



**Scheme 1.** Defect engineering route to boron nitride quantum dots (BNQDs) and edge-hydroxylated BNQDs for bioimaging. (a) Hexagonal boron nitride, (b) impinging process of heated iron nanoparticles, (c) cracks and physical defects of h-BN, (d) BNQD after microwave radiation and sonication treatments, (e) edge-hydroxylated BNQD (EH-BNQD), and (f) EH-BNQD for bioimaging.

Recently, to synthesize three-dimensional carbon nanostructures and nanohole-structured hetero-nanostructures, Oh's research group has proposed defect engineering methods using physical energy sources rather than chemical routes.<sup>28-33</sup> In those methods, atomic scale defects were intentionally produced using physical energy sources such as microwaves, lasers, and ion beams. The physical defects were used as active nucleation sites and for covalent bonding between two hetero nanostructures. Until now, physical energy sources and physical defects have not been employed to produce BNQDs from chemically inert h-BN. In this work, we report an innovative defect engineering method to synthesize blue-luminescent BNQDs and an edge-hydroxylation process to form non-toxic and biocompatible BNQDs (EH-BNQDs) that are more suitable for use in bioimaging. Initially, physical defects in h-BN were intentionally produced through an impinging process using heated iron nanoparticles, as shown in Schemes 1b and 1c. h-BN were dispersed with ferrite ( $\text{Fe}_3\text{O}_4$ ) nanoparticles in acetonitrile and annealed at 1,000 °C under nitrogen atmosphere to create cracks and holes on the h-BN surfaces. The cracked and fragmented h-BNs, as shown in Scheme 1c, were then exposed to microwave irradiation and ultrasonication to form much smaller BNQDs; this was followed by the edge-hydroxylation of the BNQDs (EH-BNQDs), for use in investigating bio-imaging applications. We observed the impinging phenomena using *in-situ* TEM: a video file of the process was recorded (Video 1) and snap shots are provided in Figure S1. We found that the interaction between h-BN layers

became weak, facilitating the formation of few-layered BN. Further, physically defective points were produced on the h-BN by the heated iron nanoparticles, and cracks were propagated by the microwave irradiation and sonication treatments, resulting in nanoscale BNQDs. The iron nanoparticles that were used in the formation of the physical defects were easily removed using a permanent magnet (Figure S1a). Furthermore, the edges of the as-synthesized BNQDs were hydroxyl-functionalized by water vapor at 900°C for 30 minutes in the furnace.<sup>27</sup> Then, the prepared BNQDs were cooled at room temperature and dispersed in water. Finally, edge-hydroxylated BNQD (EH-BNQD) was applied in bio-imaging tests. It was found that the edge-hydroxylation of the BNQDs facilitated their successful intracellular uptake for bio-imaging.

## Results and Discussion

### Morphologies of BNQDs

The development of BNQDs and defect generation on the h-BN surfaces was confirmed by morphological investigations (Figure 1). The field emission scanning electron microscopy (FESEM) image of the h-BN (Figure 1a) shows a hexagonally shaped flake with a mean thickness of about 15-20 nm, but the flakes appear to be agglomerated. After the h-BN was annealed with  $\text{Fe}_3\text{O}_4$  nanoparticles (Figures 1b and 1c), iron nanoparticles were found distributed all over the surface of the h-BN sheets. Moreover, the sheets are mostly irregular in

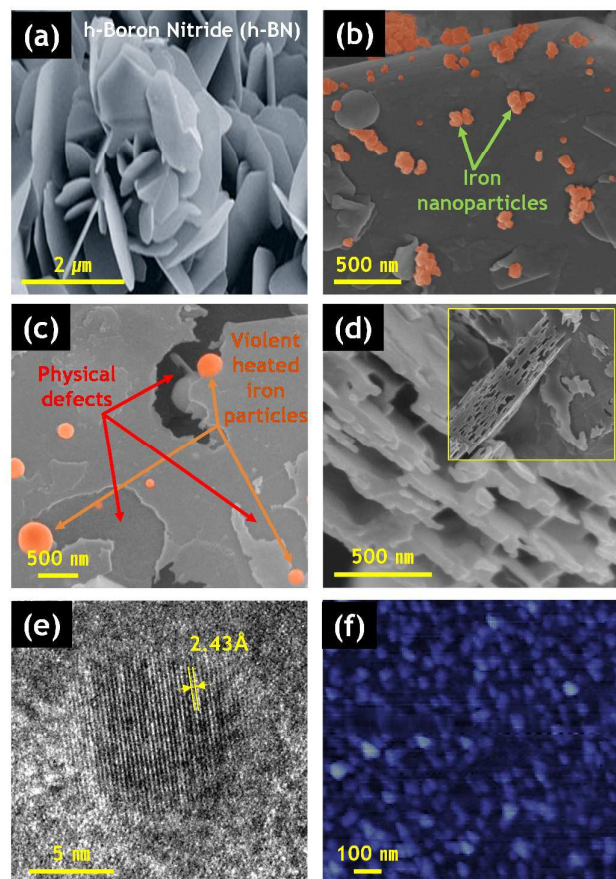


**Figure 1 Morphology of physically defected boron nitride flake and BNQDs.** (a) Hexagonal boron nitride (h-BN), (b) iron nanoparticles dispersed on h-BN, (c) SEM image of defected boron nitride flake, (d) side view of h-BN having a lot of side defects, (e) TEM image of BNQD, and (f) AFM image of BNQDs.

shape and the surfaces are smooth and planar, like the surfaces of graphene sheets, without any wrinkles.

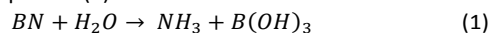
It was also clear that, physical defects were generated on the h-BN sheets by the thermal treatment because the sheets were broken not only at the edges but also on the surfaces of the h-BN flakes. Actually, in combination with the thermal energy source, the iron nanoparticles facilitated the generation this type of physical defect over all of the surfaces of the BN sheets (Figure S1). FESEM images of the top and side views of the BN sheets with generated defects after microwave irradiation (Figure 1d and the inset of Figure 1d) reveal that the thickness of the BN sheets was further reduced to a few nm and the defects were extended. This suggests that the microwave irradiation was simultaneously useful in reducing the thickness of the BN sheets as well as propagating the physical defects and cracks on the BN sheets. Notably, after sonication, BNQDs are formed, as can be confirmed in the bright field high resolution TEM (BF-HRTEM) image of the thin BNQDs (Figure 1e). As can be seen, the edges are clearly terminated, with an average size of 8 nm. The lattice fringes of 2.43 Å correspond to the (100) face of the BN crystal; this value is much smaller than that of the h-BN (002) lattice

spacing, which has a value of 3.33 Å. Additionally, the highly parallel lattice fringes indicate the BNQDs are well crystallized. Accordingly, it can be proposed that exfoliation, reduction of sheet thickness, and defect creation were achieved using physical energy sources. The fabricated BNQDs exhibited different sizes in a range from 10 nm to 50 nm; however, they were no wider than 50 nm. The height profile analysis of the BNQDs revealed that the average thickness was about 3.2 nm, signifying that the BNQDs had a few-layered structure. It is worth mentioning that the lateral size and the height profile were much more reduced than those of BN nanosheets (lateral size: 300 nm and height profile: 30 nm).<sup>26</sup>

#### Spectra analysis of BNQDs and EH-BNQDs

The crystal structures of the BNQDs and EH-BNQDs were further confirmed by Raman spectra, X-ray diffraction (XRD), X-ray photoelectron spectroscopy (XPS), and Fourier transform infrared spectroscopy (FTIR) analyses (Figure 2). The BNQDs exhibited a much weaker  $E_{2g}$  phonon mode, a counter phase B-N vibrational mode around  $1367.4\text{ cm}^{-1}$  with respect to the h-BN raw flakes. Additionally, the measured full width at half maximum (FWHM, about  $12\text{ cm}^{-1}$ ) of the BNQDs was slightly larger than that of the h-BN flakes ( $\sim 10\text{ cm}^{-1}$ ). This significant decrease in the intensity of the  $E_{2g}$  phonon mode and the slight increase of the FWHM suggest the formation of few-layered BNQDs with a decreasing in-plane lattice constant, which is in good accordance with the HRTEM findings. Interestingly, after the edge hydroxylation of the BNQDs, a much weaker  $E_{2g}$  vibrational mode appeared at  $1366.3\text{ cm}^{-1}$ , a slight red shift of about  $1\text{ cm}^{-1}$  with respect to BNQDs and h-BN, indicating a great reduction in the interlayer interaction, which leads to more exfoliation and greater formation of few layered BNQDs.<sup>27</sup> The presence of a  $sp^2$  BN structure in the BNQDs was also confirmed by FTIR spectroscopy. The sharp peaks for the h-BN flakes, located at around  $1370\text{ cm}^{-1}$  and  $785\text{ cm}^{-1}$ , correspond to the B-N vibrations in the h-BN. However, a weak peak at around  $925\text{ cm}^{-1}$  attributed to the B-O vibration is induced by the oxidation of BN. The BNQDs also show peaks similar to those of the h-BN flakes, signifying the presence of the typical  $sp^2$  bonds of BN. Interestingly, the BNQDs exhibit the  $-OH$  stretching mode at  $3220\text{ cm}^{-1}$  and a new bending mode at  $1178\text{ cm}^{-1}$  corresponding to the B-O bond, indicating that the BNQDs have a lower amount of  $-OH$  groups.<sup>27</sup> However, after the edge-hydroxylated treatment of the BNQDs, a highly intense  $-OH$  stretching signal appears at  $3360\text{ cm}^{-1}$  with the B-O bending mode at  $1271\text{ cm}^{-1}$ , confirming the successful edge-hydroxylated functionalization of the BNQDs.<sup>27</sup> X-ray powder diffraction (XRD) (Figure 2b) further revealed that the intensity of the main (002) peak at around  $26.3^\circ$  of the h-BN flakes is considerably lower for the BNQDs, indicating a reduction in the layered structure and the high exfoliation of the BNQDs after the physical defect treatments. These results agree well with the findings from the Raman spectra. Interestingly, after the edge-hydroxylation of the BNQDs, the intensity of the (002) peak was further reduced, suggesting an additional reduction in the thickness of the BN layers and more exfoliation, facilitated by the hydrolysis at

high temperature and the release of ammonia gas, as explained in Equation (1).



In this process, the hot water vapor reacts with the BNQDs, and this reaction along with the gradual weakening of the van der Waals forces between the BN layers results in the formation of voids on the (002) plane, and thereby in a reduction of the interlayer attraction forces. Additionally, *in-situ* formed  $\text{NH}_3$  penetrated through these voids, causing more exfoliation and reduction of the BN layers, as confirmed by the Raman spectra.

In order to investigate the chemical states and the quantitative chemical composition, X-ray photoelectron spectroscopy was utilized (Figures 2d-f). The XPS survey spectra of the BNQDs exhibits the typical B1s and N1s peaks, along with slight peaks of C1s and O1s, which also support the FTIR results (Figure 2c). This may be due to an ambiguous interaction that takes place during the application of physical energy sources to the h-BN flakes. The elemental percentages reveal that very low amounts of C (4.08% atomic percent) and O (7.5% atomic percent) were incorporated in the BNQDs (B 45.33% and N 43.09% atomic percent) (Table S1). The deconvoluted B1s XPS spectra of the BNQDs indicate the existence of  $\text{sp}^2$  B-N bonds (190.8 eV) and B-O bonds (192.7 eV).<sup>34</sup> The slightly higher value of the  $\text{sp}^2$  B-N bonds of the BNQDs compared to that in

h-BN (190.1 eV) may be due to the oxidation of some B atoms on the surface of the sample.<sup>35</sup> Moreover, the N1s XPS peak can be fitted to the two sub-peaks at around 398.4 eV and 400.3 eV, which correspond to the  $\text{sp}^2$  B-N bonding and C-N bonding, respectively.<sup>36</sup> Interestingly, after the edge-hydroxylated functionalization of the BNQDs, the XPS survey spectroscopy showed a large increase in the signal intensity of the O1s peak, indicating  $-\text{OH}$  groups covalently grafted to the BNQDs. Importantly, the O1s peak of the BNQDs was centered at 532.5 eV, while that of the EH-BNQDs was centered at 530.7 eV: this is an almost 1.8 eV shift, which is consistent with the edge-hydroxyl functionalization of boron nitrides.<sup>37</sup> Together, all these findings further confirm the addition of oxygen-containing functional groups to BNQDs through edge-hydroxylation.

### Optical properties of BNQDs and EH-BNQDs

The optical properties of the BNQDs and the EH-BNQDs were tested by UV-vis absorbance, photoluminescence (PL) excited by various wavelengths, and time-resolved PL (Figure 3). The absorption spectrum of the BNQDs showed a gradual increase from 600 nm, and a rapid increase at 230 nm (5.4 eV) for the bandgap of h-BN (Figure 3a). In addition, the BNQDs have a

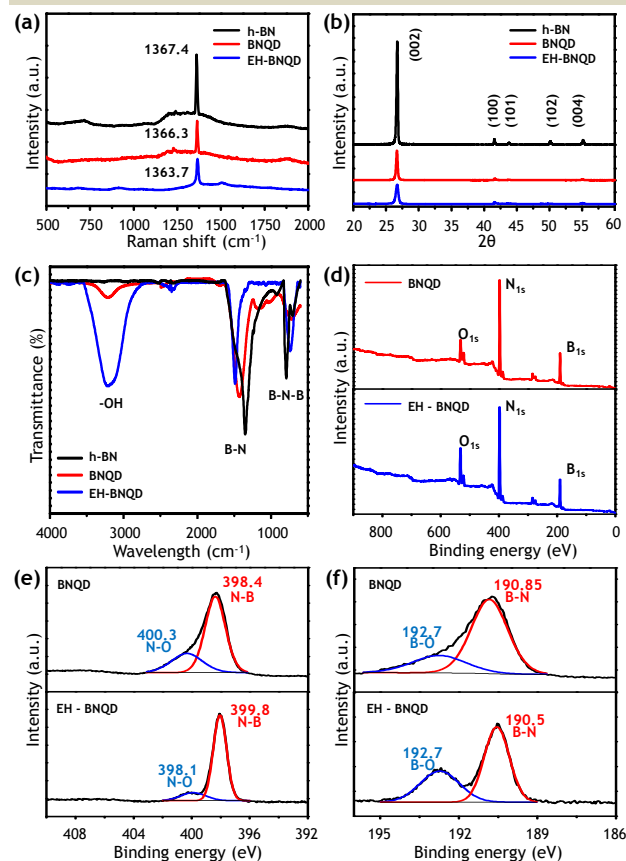


Figure 2 Chemical structures of h-BN, BNQD, and EH-BNQD; (a) Raman spectra, (b) XRD pattern, (c) FTIR measurement, and (d-f) XPS data and deconvoluted data at N1s and B1s peaks.

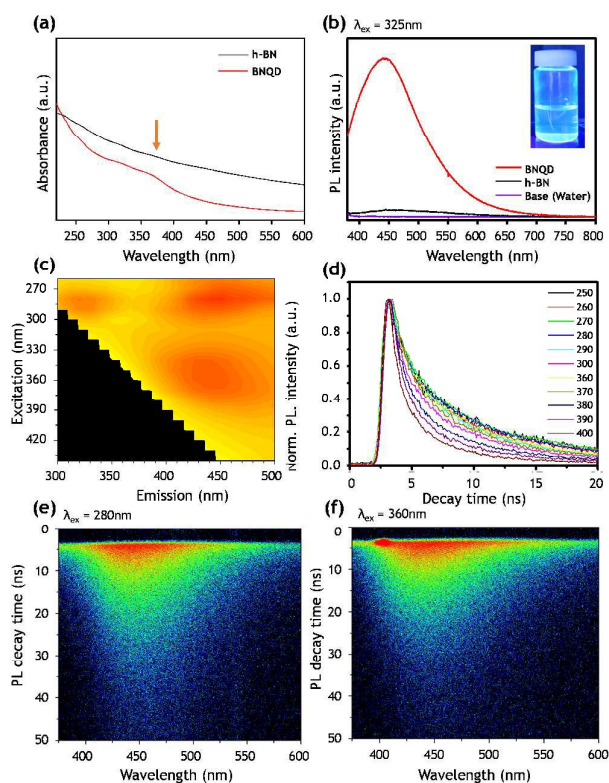


Figure 3 Optical properties of BNQDs. (a) Absorbance of BNQDs from 240 nm to 400 nm wavelength region, (b) PL spectrum of BNQDs irradiated by 325 nm He-Cd CW laser. Inset is the photograph of blue luminescent BNQDs under 365 nm UV lamp excitation, (c) Image of 2D map for PL spectra with various excitation wavelengths, (d) PL decay profiles of BNQDs for excitation from 250 nm to 400 nm, and (e, f) Streak images of time-resolved PL excited by wavelengths of 280 nm and 360 nm.

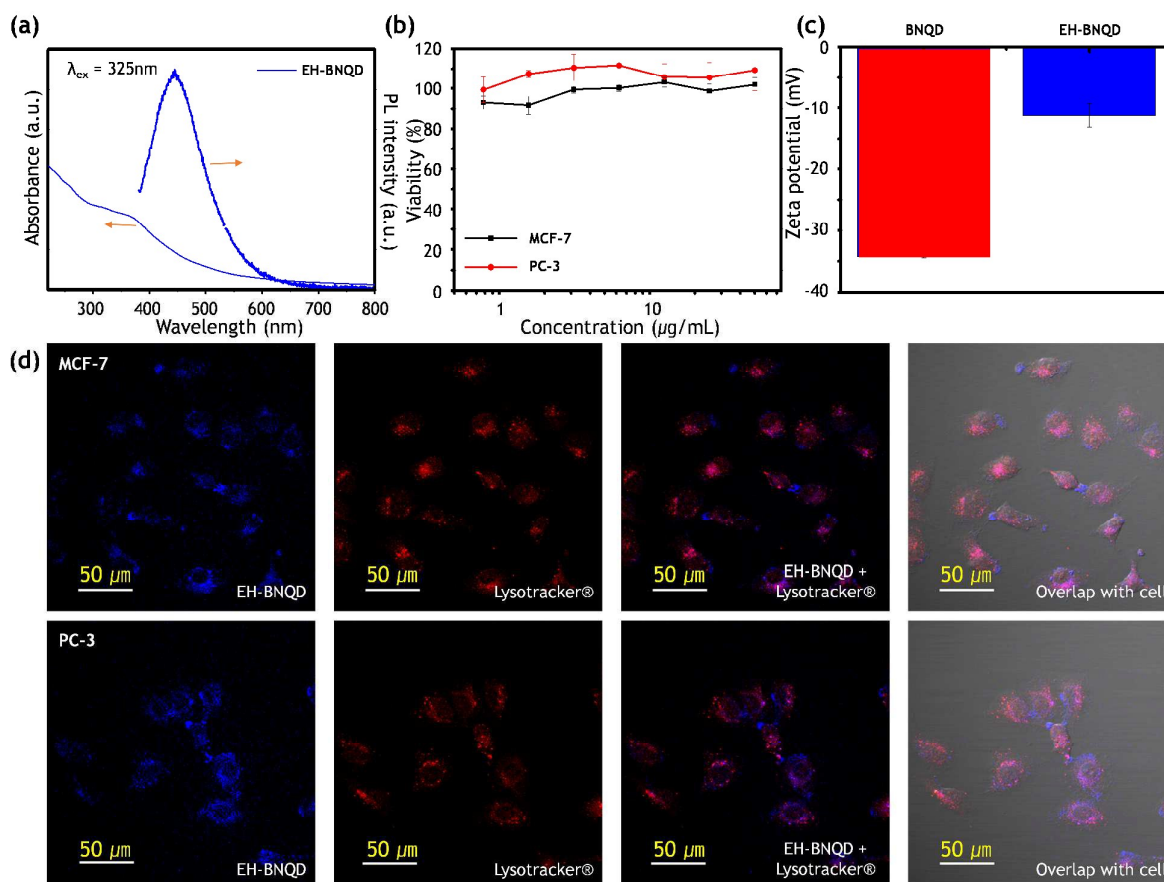


Figure 4 Application of EH-BNQDs for bioimaging. (a) UV-vis and PL of EH-BNQDs, (b) cytotoxicity of EH-BNQDs for 48 hours, (c) zeta potential of the samples, (d) confocal laser microscopic images of EH-BNQD treated MCF-7 and PC-3 cells (scale bar = 50  $\mu\text{m}$ ). EH-BNQD was colored blue and lysosome was stained with Lysotracker® (red).

shoulder peak at 280 nm which is related to several types of vacancies of nitrogen (VN) and boron (VB) in the h-BN.<sup>38</sup> When excited by a 325 nm laser source our BNQDs clearly showed a blue color light emission with a strong peak at 450 nm (Figure 3b). Normally, it is reported that visible emissions from BNQDs can be present for three reasons: N vacancy point defects, carbene structures at the zigzag edges, and  $\text{BOx}^-$  species.<sup>39</sup> For further testing, the BNQDs were separated into different particle sizes using a filtration method. However, the PL results showed an almost similar peak at 450 nm for all particle sizes (Figure S3). To further study the optical properties in the BNQDs, we measured the PL according to the change of the excitation wavelengths from 260 nm to 440 nm and plotted a 2D map of the PL (Figure 3c). The 2D map (Figure 3c) shows three emission regions, as follows: (i) a peak at 320 nm, (ii) a peak at 450 nm irradiated by the 280 nm wavelength, and (iii) a peak at 450 nm irradiated by the 360 nm wavelength. The emission at 320 nm, which is generated using an excitation at 280 nm for a shoulder peak in the UV-vis absorption, is attributed to vacancies of nitrogen (VN) and boron (VB) in the BNQDs. This emission is also observed in the h-BN bulk with various defect sites.<sup>40</sup> The PL at 450 nm shows a sensitive response to changes in the pH condition of the solvent (Figure S3). This phenomenon is related to the defect sites of oxygen,

because oxygen bonding on a 2D material is very sensitive to the pH,<sup>39, 41</sup> this was already confirmed by the presence of oxygen in the BNQDs, as determined by XPS. As a result, we consider that the emission at 450 nm comes from oxygen impurities in the BNQDs. For various excitation wavelengths, the arrangement of the PL decay curves (Figure 3d) exhibit bi-exponential profiles. They show a fast recombination time with increasing excitation wavelengths. To confirm the carrier dynamics after a pump event, we summarized the temporal profile of the time-integral PL (TIPL) (Figures 3e, 3f). As time passes, the TIPL irradiated by 270 nm and 360 nm exhibits a slight spectral migration (Figure S4). The sharp peaks indicate the Raman spectra for DI water solvent, similar to cases found in the literature on graphene quantum dots (Figure 3f).<sup>42, 43</sup> These results indicate that the presence of a single luminescence origin comes from the defect sites formed by oxygens. Furthermore, the quantum yields (QYs) of the BNQDs and EH-BNQDs were measured by using quinine sulfate as a reference.<sup>44, 45</sup> The PL quantum yield of quinine sulfate was 54.60% as calculated. As a result, the average QY of BNQDs was  $1.19 \pm 0.34\%$  and the EH-BNQDs was 0.7% for the highest QY. In this result, the QY of EH-BNQDs was decreased, since the defect sites were reduced by hydroxylate groups. However,

the hydroxylate groups cause the surface charge to be slightly negative, which is acceptable for uptake by cells (Figure 4b).

#### Bio-imaging test of BNQDs and EH-BNQDs

In bio-imaging, it is important that the bio-imaging agent does not influence the viability of the target cell or tissue. The UV-vis and PL intensity of the EH-BNQDs irradiated by 325 nm wavelength are shown in Figure 4a. The cytotoxicity of the EH-BNQD was evaluated by MTT assay (Figure 4b). The viabilities of MCF-7 (human breast cancer cell) and PC-3 (human prostate cancer cell) against EH-BNQDs were around 100 % for the overall concentration range, indicating that EH-BNQD itself is non-toxic and can be applied as a bio-imaging agent. The cytotoxicity of BNQDs against HeLa cells for 48 hours was about 80% (Figure S5). It is widely known that having a suitable size and zeta potential are prerequisite properties for the introduction of a nanomaterial as a bio-imaging agent. In this case, the surface charge was slightly negative, which is acceptable for uptake by cells (Figure 4b). The intracellular fluorescence of the EH-BNQD was observed by confocal laser scanning microscopy (CLSM) against MCF-7 and PC-3 cells (Figure 4c). A significant blue fluorescence was observed in the perinuclear region; this fluorescence is thought to be the result of endocytosis. In order to ensure the uptake of EN-BNQD, the intracellular endosome was labeled with LysoTracker® (red) and the localization was compared with the fluorescence of the EH-BNQD (blue). The blue signal of the EH-BNQD and the red signal of LysoTracker® overlapped into the purple color, which implies the successful endocytosis of EH-BNQD (Figure 4d). Because the edge hydroxyl groups are favored for modification by other functional moieties such as cell specific ligands or delivery carriers, further biological applications including bio-imaging are highly anticipated.

#### Conclusions

We report the development of a defect engineering method for synthesizing boron nitride quantum dots (BNQDs) from chemically inert h-BN using physical energy sources, and a further functionalization process to fabricate biocompatible edge-hydroxylated BNQDs (EH-BNQDs) for bioimaging. Physical defects were intentionally produced on chemically inert h-BN using an impinging process of heated iron nanoparticles, and micro-cracks were further propagated using microwave radiation and sonication treatments, resulting in much smaller and few-layered BNQDs. Edge-hydroxylated functionalization was performed to enhance the biocompatibility and cell adhesion of the BNQDs. The experimental results showed that the EH-BNQDs exhibited a blue colored photoluminescence with 325nm laser excitation, very good cytotoxicity with approximately 100% cell viability, and a good attachment to cell surfaces. We also demonstrated the successful endocytosis of EH-BNQDs using a cancer cell line.

#### Experimental

#### Syntheses of BNQDs and EH-BNQDs

Physical defects were intentionally produced in h-BN through an impinging process of heated iron nanoparticles. h-BN and ferrite (Fe<sub>3</sub>O<sub>4</sub>) nanoparticles were dispersed in acetonitrile and annealed at 1,000 °C under nitrogen atmosphere to create cracks and holes on the h-BN surfaces. Furthermore, physically defective points were produced on h-BN by heated iron nanoparticles, and cracks were propagated, using microwave irradiation and sonication treatments, resulting in nanoscale BNQDs. The iron nanoparticles that were used for the formation of the physical defects were easily removed using a permanent magnet. The edges of the as-synthesized BNQDs were then hydroxyl-functionalized using water vapor at 900°C for 30 minutes in a furnace. The edge-hydroxylated BNQDs (EH-BNQDs) were then cooled at room temperature and dispersed in water prior to use in experimental tests to explore their properties in bio-imaging applications.

#### Materials

Commercially available boron nitride flakes and iron nanoparticles, and thiazolyl blue tetrazoliumbromide (MTT) were purchased from Sigma Aldrich (St. Louis, MO). LysoTracker® Red DND-99 was purchased from Invitrogen (MA). All of the materials were used as purchased.

#### Instrumental methods

The morphologies were examined using SEM (NOVA230) and TEM (Tecnai G2 F30 S-Twin). The height of the BNQDs was measured using AFM (N8 NEOS Senterra) in non-contact mode. High-resolution X-ray photoelectron spectroscopy (XPS) results were determined using an ESCA Multilab 200 system. Raman spectra were obtained with an ARAMIS High Power Normal & Micro X-ray Diffractometer (D/MAX-2500(18kW), RIGAKU), Multi-Purpose X-Ray Photoelectron Spectroscopy (XPS) (Sigma Probe, Thermo VG Scientific), and FT-IR Spectrometer (FT-IR 4100, Jasco). Monochromatic light from a 300 W xenon lamp, dispersed by a monochromator, was focused on the samples for the PL and PLE experiments at low-excitation power (< 0.1 mW) at room temperature. The PL and PLE spectra were detected by a UV spectrometer (Maya2000, Ocean Optics, USA) and a highly-sensitive photomultiplier tube detector at room temperature. A mode-locked femto-second pulsed Ti:sapphire laser (Coherent, Chameleon Ultra II) system was used as the excitation source; three wavelengths of the pulsed Ti:sapphire laser (300 nm, 370 nm, and 470 nm) were employed. A streak camera (Hamamatsu, C7700-01) was utilized to measure the decay profile of the PL spectra at room temperature. TEM image were taken using a transmission electron microscope (JEM-2210, JEOL) and analyzed using a Gatan Digital Microscope. Fluorescence spectra were measured using a spectrofluorophotometer (RF-5301 PC, Shimadzu). Zeta potential was measured using a zetasizer (Nano Z, Malvern) at 0.1 mg/mL in PBS. The confocal laser scanning microscope (CLSM) image was obtained using an Olympus FV-1000 and analyzed using OLYMPUS FLUOVIEW ver. 1.7 Viewer software.

#### Cell viability test

The dose-dependent cytotoxicity of the EH-BNQDs were measured. Cells (MCF-7 and PC-3) were seeded on a 96 well culture plate at a density of 8000 cells/well and incubated overnight. MCF-7 (human breast adenocarcinoma cell line, KCLB30022) and PC-3 (human postate adenocarcinoma cell line, KCLB21435) were obtained from the Korea Cell Line Bank (KCLB). The medium was replaced with fresh medium containing 0 to 50 µg/mL of EH-BNQD, and the cells were further incubated for 24 h. After incubation, cell viability was evaluated by MTT assay.

For the MTT assay, the medium was replaced with 180 µL of fresh medium and 20 µL of MTT solution (5 mg/mL) was added. After incubation in the dark for 4 h, the medium was removed and purple crystals were completely dissolved in 200 µL of DMSO. 100 µL of each solution was transferred into a new 96 well plate and the UV-vis absorbance at 570 nm was measured using a microplate spectrofluorometer (VICTOR3 V multilabel counter). The relative percentages of non-treated cells were used to represent 100 % cell viability.

#### Bio-imaging by confocal laser scanning microscopy (CLSM)

Intracellular BN was observed by confocal microscopy image. Briefly, MCF-7 or PC-3 cells (80,000 cells/well) were seeded on the glass cover slips, placed in a 12 well culture plate, and incubated overnight. Then, the medium was replaced with fresh serum-free medium containing 50 µg/mL EH-BNQD; after 4 h of incubation, the cells were washed carefully with PBS. Then, Lysotracker® red DND-99 was employed at a final concentration of 4 µM and the cells were further incubated for 5 minutes; the cells were then washed carefully with PBS. Finally, the cells were fixed with 10 % neutrally buffered formalin (NBF) at 4 °C overnight. The cells on the coverslip were mounted in Vectashield anti-fade mounting medium for fluorescence measurement (Vector Labs) and were observed by CLSM. The EH-BNQD was monitored by 405/425-475 nm, and Lysotracker was monitored by 543/550-650 nm, and they were pseudo-colored as blue and red, respectively.

#### Acknowledgements

This work was partially supported by Creative Research Initiative Program (2015R1A3A2028975), funded by National Research Foundation of Korea (NRF).

#### References

- 1 A. Zunger, A. Katzir, A. Halperin, *Phys. Rev. B*, 1976, **13**, 5560.
- 2 K. Watanabe, T. Taniguchi, H. Kanda, *Nat. Mater.*, 2004, **3**, 404-409.
- 3 Z. Zhang, W. Guo, *J. Phys. Chem. Lett.*, 2011, **2**, 2168-2173.
- 4 C. Zhi, Y. Bando, C. Tang, H. Kuwahara, D. Golberg, *Adv. Mater.*, 2009, **21**, 2889-2893.
- 5 L. H. Li, J. Cervenka, K. Watanabe, T. Taniguchi, Y. Chen, *ACS Nano*, 2014, **8**, 1457-1462.
- 6 Y. Lin, J. W. Connell, *Nanoscale*, 2012, **4**, 6908-6939.
- 7 P. Sutter, J. Lahiri, P. Zahl, B. Wang, E. Sutter, *Nano Lett.*, 2012, **13**, 276-281.
- 8 Y. Yabe, T. Yamada, S. Nagata, Y. Sawama, Y. Monguchi, H. Sajiki, *Adv. Syn. Cat.*, 2012, **354**, 1264-1268.
- 9 M. Bernardi, M. Palumbo, J. C. Grossman, *Phys. Rev. Lett.*, 2012, **108**, 226805.

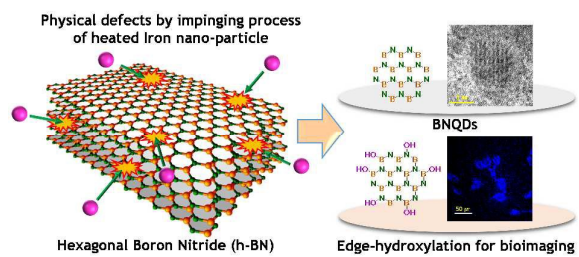
- 10 J. Wu, B. Wang, Y. Wei, R. Yang, M. Dresselhaus, *Mater. Res. Lett.*, 2013, **1**, 200-206.
- 11 T. Han, Y. Luo, C. Wang, *J. Phys. D: Appl. Phys.*, 2014, **47**, 025303.
- 12 Y. Kubota, K. Watanabe, O. Tsuda, T. Taniguchi, *Science*, 2007, **317**, 932-934.
- 13 M. Yi, Z. Shen, X. Zhao, S. Liang, L. Liu, *Appl. Phys. Lett.*, 2014, **104**, 143101.
- 14 R. Kumar, K. Gopalakrishnan, I. Ahmad, C. Rao, *Adv. Funct. Mater.*, 2015, **25**, 5910-5917.
- 15 S. Umrao, M.-H. Jang, J.-H. Oh, G. Kim, S. Sahoo, Y.-H. Cho, A. Srivastava, I.-K. Oh, *Carbon*, 2015, **81**, 514-524.
- 16 J. Shen, Y. Zhu, X. Yang, C. Li, *Chem. Commun.*, 2012, **48**, 3686-3699.
- 17 Y. Li, Y. Hu, Y. Zhao, G. Shi, L. Deng, Y. Hou, L. Qu, *Adv. Mater.*, 2011, **23**, 776-780.
- 18 D. I. Son, B. W. Kwon, D. H. Park, W.-S. Seo, Y. Yi, B. Angadi, C.-L. Lee, W. K. Choi, *Nat. Nanotechnol.*, 2012, **7**, 465-471.
- 19 V. Gupta, N. Chaudhary, R. Srivastava, G. D. Sharma, R. Bhardwaj, S. Chand, *J. Am. Chem. Soc.*, 2011, **133**, 9960-9963.
- 20 P. G. Luo, S. Sahu, S.-T. Yang, S. K. Sonkar, J. Wang, H. Wang, G. E. LeCroy, L. Cao, Y.-P. Sun, *J. Mater. Chem. B*, 2013, **1**, 2116-2127.
- 21 C. Wu, C. Wang, T. Han, X. Zhou, S. Guo, J. Zhang, *Adv. Healthcare Mater.*, 2013, **2**, 1613-1619.
- 22 R. Kumar, A. Parashar, *Nanoscale*, 2016, **8**, 22-49.
- 23 A. Fedorov, C. Praveen, N. Verbitskiy, D. Haberer, D. Usachov, D. Vyalikh, A. Nefedov, C. Wöll, L. Petaccia, S. Piccinin, *Phys. Rev. B*, 2015, **92**, 125440.
- 24 L. Lin, Y. Xu, S. Zhang, I. M. Ross, A. C. Ong, D. A. Allwood, *ACS Nano*, 2013, **7**, 8214-8223.
- 25 L. Lin, Y. Xu, S. Zhang, I. M. Ross, A. C. Ong, D. A. Allwood, *Small*, 2014, **10**, 60-65.
- 26 Z. Lei, S. Xu, J. Wan, P. Wu, *Nanoscale*, 2015, **7**, 18902-18907.
- 27 F. Xiao, S. Naficy, G. Casillas, M. H. Khan, T. Katkus, L. Jiang, H. Liu, H. Li, Z. Huang, *Adv. Mater.*, 2015, **27**, 7196-7203.
- 28 V. Sridhar, H.-J. Kim, J.-H. Jung, C. Lee, S. Park, I.-K. Oh, *ACS Nano*, 2012, **6**, 10562-10570.
- 29 R. Kumar, J.-H. Oh, H.-J. Kim, J.-H. Jung, C.-H. Jung, W. G. Hong, H.-J. Kim, J.-Y. Park, I.-K. Oh, *ACS Nano*, 2015, **9**, 7343-7351.
- 30 H. J. Kim, H. Randriamahazaka, I. K. Oh, *Small*, 2014, **10**, 5023-5029.
- 31 S.-H. Lee, V. Sridhar, J.-H. Jung, K. Karthikeyan, Y.-S. Lee, R. Mukherjee, N. Koratkar, I.-K. Oh, *ACS Nano*, 2013, **7**, 4242-4251.
- 32 S.-H. Bae, K. Karthikeyan, Y.-S. Lee, I.-K. Oh, *Carbon*, 2013, **64**, 527-536.
- 33 S. Vadahanambi, S.-H. Lee, W.-J. Kim, I.-K. Oh, *Environ. Sci. Tech.*, 2013, **47**, 10510-10517.
- 34 A. S. Nazarov, V. N. Demin, E. D. Grayfer, A. I. Bulavchenko, A. T. Arymbaeva, H. J. Shin, J. Y. Choi, V. E. Fedorov, *Chem. Asian J*, 2012, **7**, 554-560.
- 35 A. Pakdel, X. Wang, C. Zhi, Y. Bando, K. Watanabe, T. Sekiguchi, T. Nakayama, D. Golberg, *J. Mater. Chem.*, 2012, **22**, 4818-4824.
- 36 N. Tripathi, M. Yamashita, T. Akai, *J. Mater. Chem. C*, 2014, **2**, 622-625.
- 37 H. Sachdev, F. Müller, S. Hüfner, *Diamond Relat. Mater.*, 2010, **19**, 1027-1033.
- 38 C. Attacalite, M. Bockstedte, A. Marini, A. Rubio, L. Wirtz, *Phys. Rev. B*, 2011, **83**, 144115.
- 39 L. Lin, Y. Xu, S. Zhang, I. M. Ross, A. Ong and D. A. Allwood, *Small*, 2014, **10**, 60-65.
- 40 V. Solozhenko, A. Lazarenko, J.-P. Petit, A. Kanaev, *J. Phys. Chem. Sol.*, 2001, **62**, 1331-1334.

## ARTICLE

Journal Name

- 41 W. Fu, C. Nef, O. Knopfmacher, A. Tarasov, M. Weiss, M. Calame, C. Schönenberger, *Nano Lett.*, 2011, **11**, 3597-3600.
- 42 S. H. Song, M. H. Jang, J. Chung, S. H. Jin, B. H. Kim, S. H. Hur, S. Yoo, Y. H. Cho, S. Jeon, *Adv. Opt. Mater.*, 2014, **2**, 1016-1023.
- 43 M. H. Jang, H. D. Ha, E. S. Lee, F. Liu, Y. H. Kim, T. S. Seo, Y. H. Cho, *Small*, 2015, **11**, 3773-3781.
- 44 D. Pant, U. C. Tripathi, G. C. Joshi, H. B. Tripathi and D. D. Pant, *J. Photochem. Photobiol. A: Chem*, 1990, **51**, 313-325.
- 45 M. Li, W. Wu, W. Ren, H. Cheng, N. Tang, W. Zhong and Y. Du, *Appl. Phys. Lett*, 2012, **101**, 103107

## Table of contents



Defect engineering method was developed using physical energy sources to synthesize boron nitride quantum dots (BNQDs) for their bioimaging applications.